



Shanghai Institute of Technical Physics



Modeling of dark characteristics for long-wavelength HgCdTe photodiode

Z. J. Quan, X. S. Chen, W. Lu

National Laboratory for Infrared Physics
Shanghai Institute of Technical Physics
Chinese Academy of Sciences



Outline

- Introduction
- Carrier density approximation
- Fitting method
- Error analysis for extracted parameters
- Some Application
- Conclusion



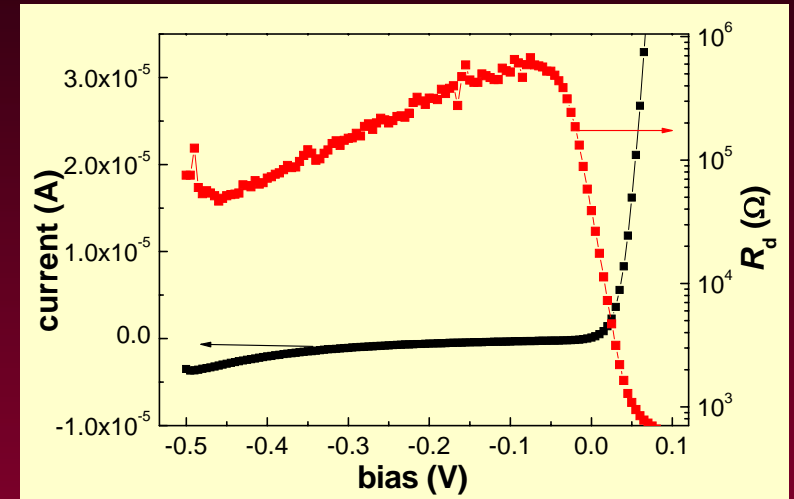
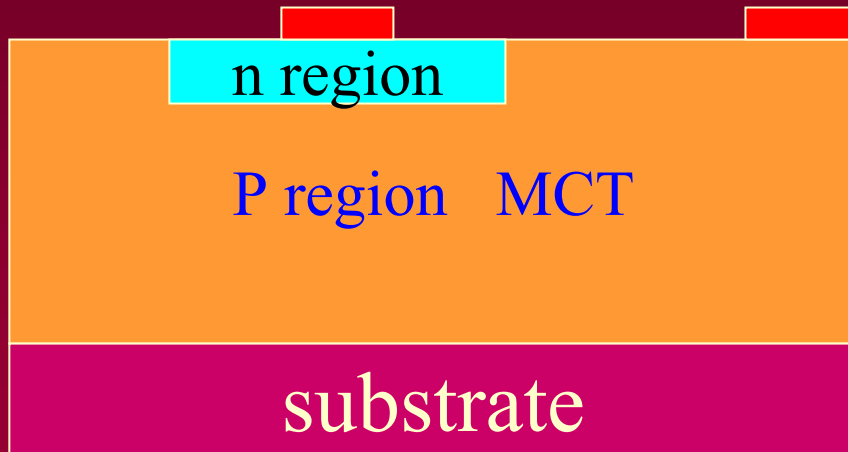
Introduction

HgCdTe (Mercury Cadmium Telluride, MCT) has been proven to be the most versatile and highest performing semiconductor material for the fabrication of infrared (IR) detectors.

Since the realization of MCT devices is a complicated and expensive fabrication process, device simulation has become a critical tool for the development of MCT devices.



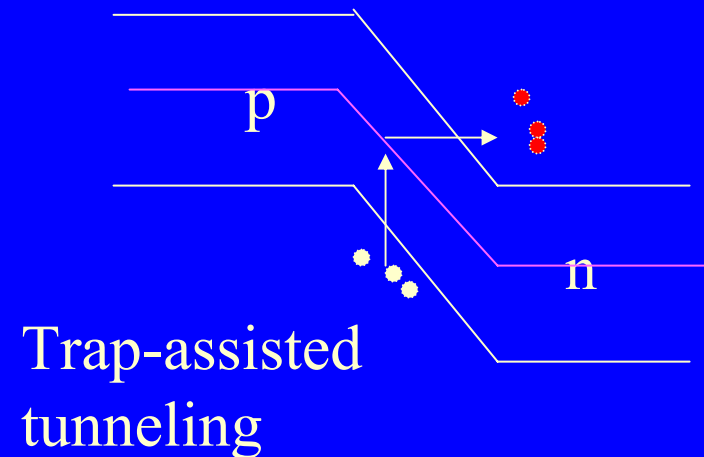
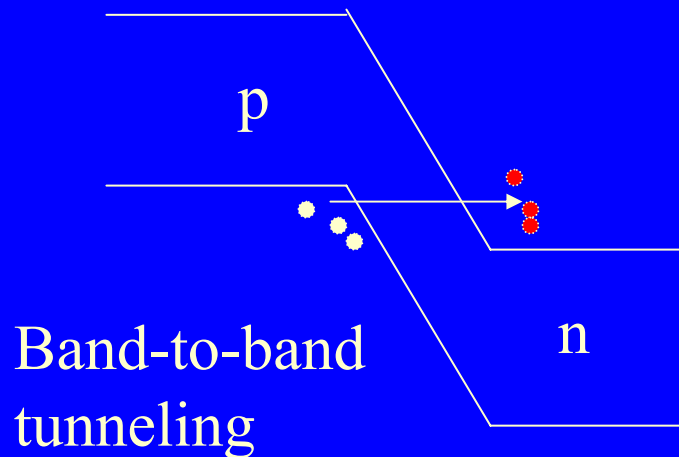
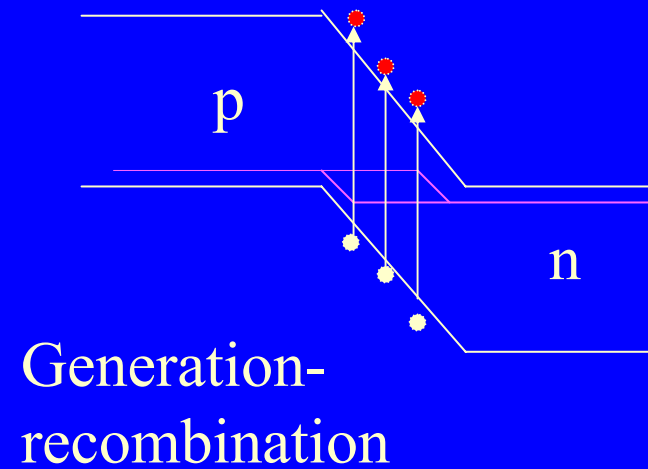
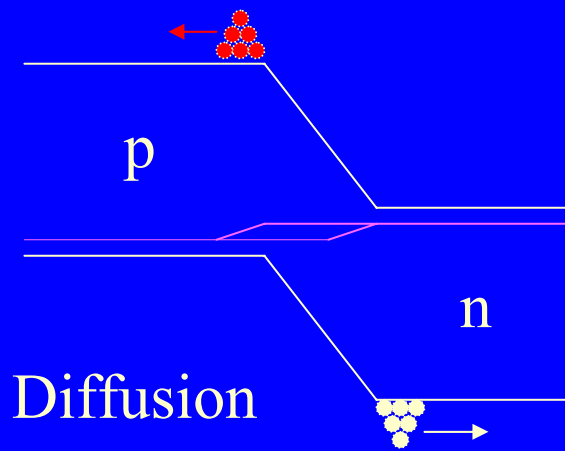
The structure of n-on-p devices whose junction is formed by ion implantation:



Extracting parameters from the I-V curves and R-V curves and revealing roles of the different physical mechanisms.



Dark current mechanisms of MCT devices:





The expressions of analytic model:

$$J_{diff} = qn_i^2 \sqrt{\frac{kT}{q}} \left(\sqrt{\frac{\mu_n}{\tau_n}} \cdot \frac{1}{N_a} + \sqrt{\frac{\mu_p}{\tau_p}} \cdot \frac{1}{N_d} \right) \left(\exp\left(\frac{qV_d}{kT}\right) - 1 \right)$$

Diffusion

$$J_{gr} = \frac{n_i W_0 kT}{\tau_0 V_{bi}} \frac{2 \sinh\left(\frac{qV_d}{2kT}\right)}{\left(1 - \frac{V_d}{V_{bi}}\right)^{\frac{1}{2}}} \cdot f(b)$$

Generation-recombination

$$J_{BBT} = \frac{q^3 \sqrt{2m_e^*} E(V_{bi} - V_d)}{4\pi^2 \hbar^2 \sqrt{E_g}} \exp\left(-\frac{\pi \sqrt{m_e^* / 2E_g^{3/2}}}{2qE\hbar}\right)$$

Band-to-band
tunneling

$$J_{TAT} = \frac{\pi^2 q^2 N_t m_e^* M^2 (V_{bi} - V_d)}{h^3 (E_g - E_t)} \exp\left(-\frac{\sqrt{3} E_g^2 F(a)}{8\sqrt{2} qPE}\right)$$

Trap-assisted
tunneling



However, MCT is a narrow bandgap semiconductor that exhibits a non-parabolic conduction band and high carrier degeneracy.

Practically understanding of carrier degeneracy and conduction band non-parabolicity effects on the simulation of MCT photovoltaic devices

and establishing a simple carrier density approximation that takes account of the two factors in simulation

will be greatly beneficial to the design, analysis and characterization of MCT devices.



Carrier density approximation

The general carrier density can be expressed by

$$n = \int \frac{dN}{dE} \cdot f(E) \cdot dE$$

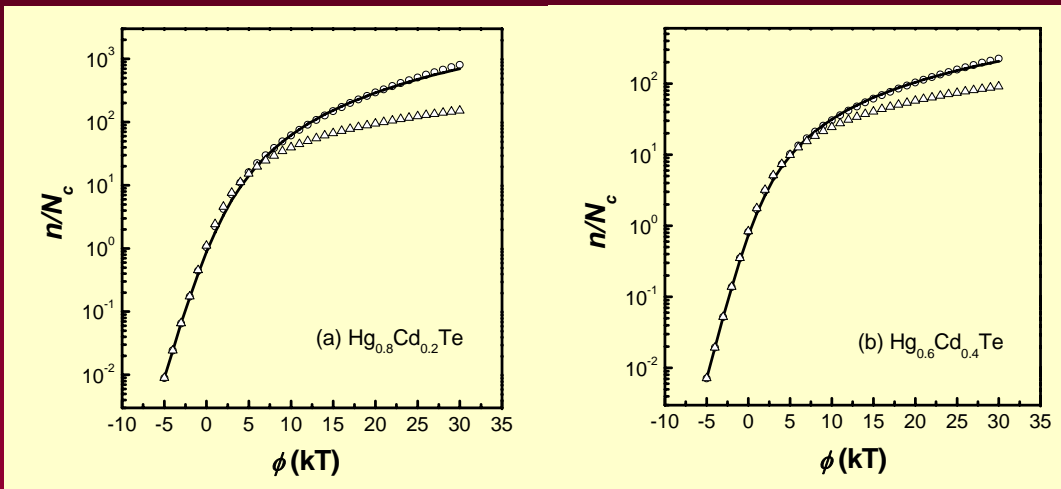
by considering both carrier degeneracy and conduction band non-parabolicity, the carrier density is given by the following integral expression

$$n = \frac{2N_c}{\sqrt{\pi}} \int_0^\infty \frac{\varepsilon^{1/2} (1 + \alpha\varepsilon)^{1/2} (1 + 2\alpha\varepsilon)}{\exp(\varepsilon - \phi) + 1} d\varepsilon$$



we propose a new simple carrier approximation derived from the Ariel model, adding three parameters α_1 , α_2 and B_2 as follows:

$$\phi = \ln \frac{n}{B_0 N_c} + B_1 \left(\frac{n}{N_c} \right)^{\alpha_1} + B_2 \left(\frac{n}{N_c} \right)^{\alpha_2}$$



As can be seen, our new approximation is in good agreement with the numerical solution in the range of $\phi < 30$ for both LWIR and MWIR devices.

Comparisons of carrier concentration versus reduced Fermi level in the range of $\phi < 30$ for $\text{Hg}_{0.8}\text{Cd}_{0.2}\text{Te}$ (a), and $\text{Hg}_{0.6}\text{Cd}_{0.4}\text{Te}$ (b) at 80 K calculated by actual numerical solution (open circle), Ariel model (open triangle), and the approximation Eq. (3a) (solid lines) in Model I (carrier degeneracy and conduction band non-parabolicity)



An implicit expression for n_i can be obtained, This equation can be solved iteratively for n_i if the other quantities are known.

$$\frac{n_i^2}{B_0 B_{0v}} \exp \left[B_1 \left(\frac{n_i}{N_c} \right)^{\alpha_1} + B_2 \left(\frac{n_i}{N_c} \right)^{\alpha_2} + B_{1v} \left(\frac{n_i}{N_v} \right)^{\alpha_{1v}} + B_{2v} \left(\frac{n_i}{N_v} \right)^{\alpha_{2v}} \right] = N_c N_v \exp(-\varepsilon_g)$$

We obtain the following expression for the intrinsic Fermi level ϕ_i of a non-parabolic semiconductor:

$$\phi_i = -\frac{\varepsilon_g}{2} + \frac{1}{2} \ln \left(\frac{B_{0v} N_v}{B_0 N_c} \right) + \frac{1}{2} \left[B_1 \left(\frac{n_i}{N_c} \right)^{\alpha_1} + B_2 \left(\frac{n_i}{N_c} \right)^{\alpha_2} - B_{1v} \left(\frac{n_i}{N_v} \right)^{\alpha_{1v}} - B_{2v} \left(\frac{n_i}{N_v} \right)^{\alpha_{2v}} \right]$$



With known n_i , ϕ_i , and with the help of Eq. (3), we derive new relations that describe the Fermi level in terms of carrier densities and intrinsic properties:

$$\phi_n - \phi_i = \ln\left(\frac{n}{n_i}\right) + B_1 \left[\left(\frac{n}{N_c}\right)^{\alpha_1} - \left(\frac{n_i}{N_c}\right)^{\alpha_1} \right] + B_2 \left[\left(\frac{n}{N_c}\right)^{\alpha_2} - \left(\frac{n_i}{N_c}\right)^{\alpha_2} \right]$$

$$\phi_i - \phi_p = \ln\left(\frac{p}{n_i}\right) + B_{1v} \left[\left(\frac{p}{N_v}\right)^{\alpha_{1v}} - \left(\frac{n_i}{N_v}\right)^{\alpha_{1v}} \right] + B_{2v} \left[\left(\frac{p}{N_v}\right)^{\alpha_{2v}} - \left(\frac{n_i}{N_v}\right)^{\alpha_{2v}} \right]$$

The expression can be solved iteratively for Fermi level E_{fn} and E_{fp} , which are the Fermi energy level of the n -side and the p -side without contact with each other. So we can obtain the built-in potential $V_{bi} = E_{fn} - E_{fp}$ of the p - n junction.

Non-parabolicity and carrier degeneracy can be adequately modeled by the calculation of built-in potential V_{bi} , intrinsic carrier concentration n_i and intrinsic Fermi level E_i .



Effects of carrier degeneracy and conduction band non-parabolicity?

- (I) The carrier degeneracy and the conduction band non-parabolicity (above carrier density approximation)

$$\phi = \ln \frac{n}{B_0 N_c} + B_1 \left(\frac{n}{N_c} \right)^{\alpha_1} + B_2 \left(\frac{n}{N_c} \right)^{\alpha_2}$$

- (II) Only the carrier degeneracy

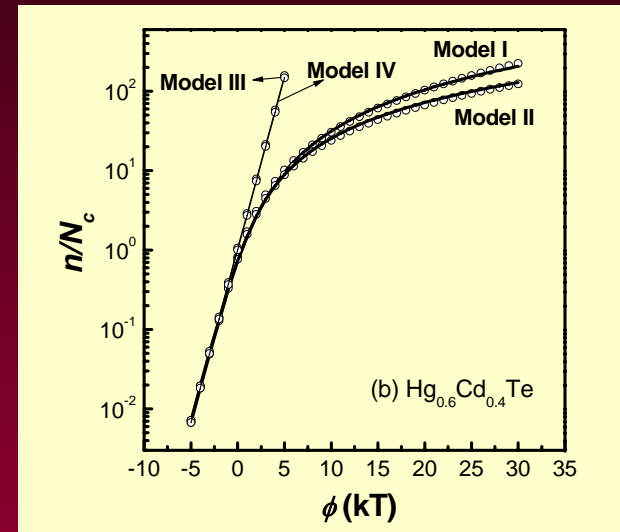
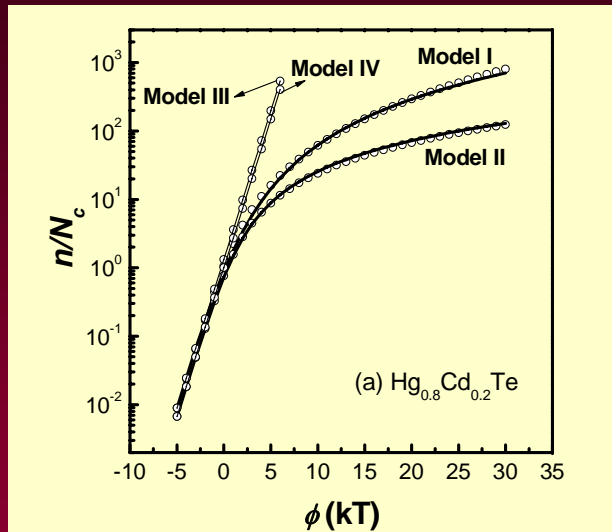
$$\phi = \ln \frac{n}{N_c} + 0.994 \left(\frac{n}{N_c} \right)^{0.745} - 0.577 \left(\frac{n}{N_c} \right)^{0.624}$$

- (III) Only the conduction band non-parabolicity

$$n = B_0 N_c \exp(\phi)$$

- (IV) Neither of these two factors.

$$n = N_c \exp(\phi)$$



Calculated carrier concentration versus reduced Fermi level with four models for $\text{Hg}_{0.8}\text{Cd}_{0.2}\text{Te}$ (a), and $\text{Hg}_{0.6}\text{Cd}_{0.4}\text{Te}$ (b) at 80 K (solid lines). The actual numerical solutions (open circles).



Model I, Model II underestimates the carrier density, while Model III and Model IV yield significantly larger carrier density at the range of $\phi > 0$.

When Cd composition x changes from 0.2 to 0.4, the difference between Model I and Model II decreases because the increased bandgap decreases the non-parabolicity factor α .

The calculations (solid lines) fit accurately the corresponding numerical solutions (open circles), respectively, for $\phi < 30$.

Indicating that these models can be used in place of numerical solution to investigate the effects of carrier degeneracy and conduction band non-parabolicity on the simulation of MCT photovoltaic devices.



To further verify the applicability of the above approximations, the measured R_d - V curves from real MCT devices are fitted with the analytic model by using the four approximations.

Table I. Material and device parameters of the two MCT photovoltaic samples used for measuring R_d - V curves

	x	T (K)	A (cm ²)	N_a (cm ⁻³)	μ_p (cm ² /Vs)
Sample I	0.2323	80	2.5×10^{-5}	5.65×10^{15}	813
Sample II	0.2927	80	2.5×10^{-5}	4.66×10^{15}	579

Table II. Fitting parameters obtained by fitting the four models to the measured R_d - V curves of Sample I

Model	μ_p/τ_n (cm ² /Vs ²)	τ_0 (ns)	N_d (cm ⁻³)	E_v/E_g	N_t (cm ⁻³)
I	1.613×10^{14}	0.154	1.493×10^{16}	0.486	1.659×10^{12}
II	2.128×10^{14}	0.121	1.478×10^{16}	0.488	1.624×10^{12}
III	1.096×10^{14}	0.142	1.564×10^{16}	0.488	1.721×10^{12}
IV	1.248×10^{14}	0.119	1.543×10^{16}	0.488	1.722×10^{12}

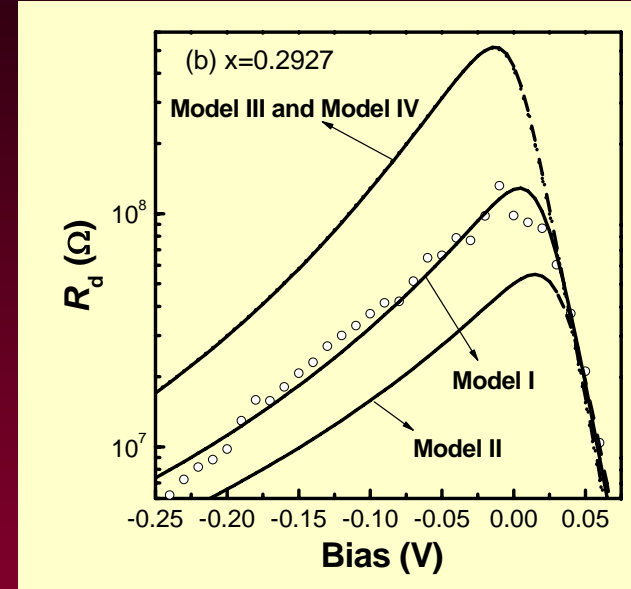
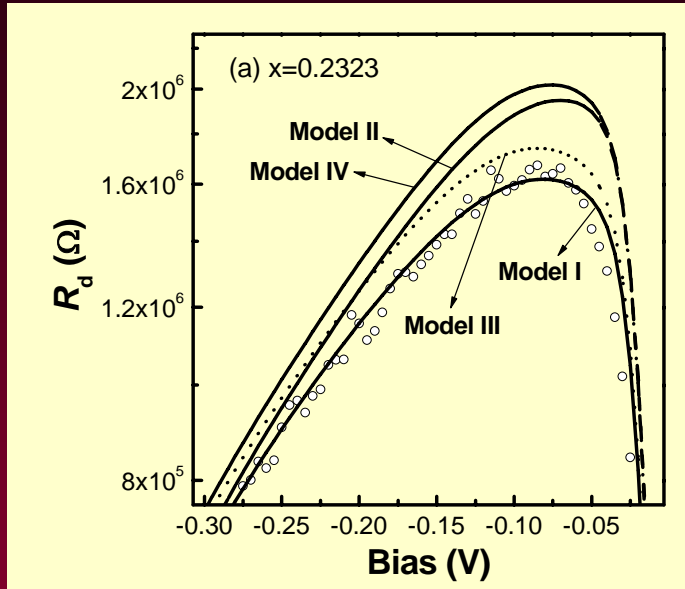
Table III. Fitting parameters obtained by fitting the four models to the measured R_d - V curves of Sample II

Model	τ_0 (ns)	N_d (cm ⁻³)	E_v/E_g	N_t (cm ⁻³)
I	1.488	8.649×10^{17}	0.586	1.302×10^{13}
II	1.389	4.759×10^{17}	0.589	1.174×10^{13}
III	1.492	1.0×10^{19}	0.581	4.398×10^{13}
IV	1.492	1.0×10^{19}	0.581	4.398×10^{13}



It is evident from these tables that these parameters from the four models are different from each other, and the sensitivity of the fitted values of device parameters to the used model is obvious.

This implies that the omission of carrier degeneracy and conduction band non-parabolicity brings deviations into the simulation of MCT device, and the magnitude of the deviations is dependent on the parameters of device and material.



To estimate the deviation of R_d - V characteristics calculated by Model II, III and IV from those calculated using Model I, all the parameters in Table I and the parameters for Model I in Table II and III are also employed in the further calculations. The calculated results are also shown in Figure 3. It is evident from the figure that, comparing with Model I, Model II predicts larger R_d for LWIR ($x=0.2323$) and smaller R_d for MWIR ($x=0.2927$), while Model III and Model IV yield larger R_d for both LWIR and MWIR.



The differences of the built-in potential V_{bi} , the intrinsic carrier concentration n_i and the intrinsic Fermi level E_i are responsible for the differences in the above three R_d - V curves. It is that the carrier degeneracy and the conduction band nonparabolicity influence the simulation calculations.

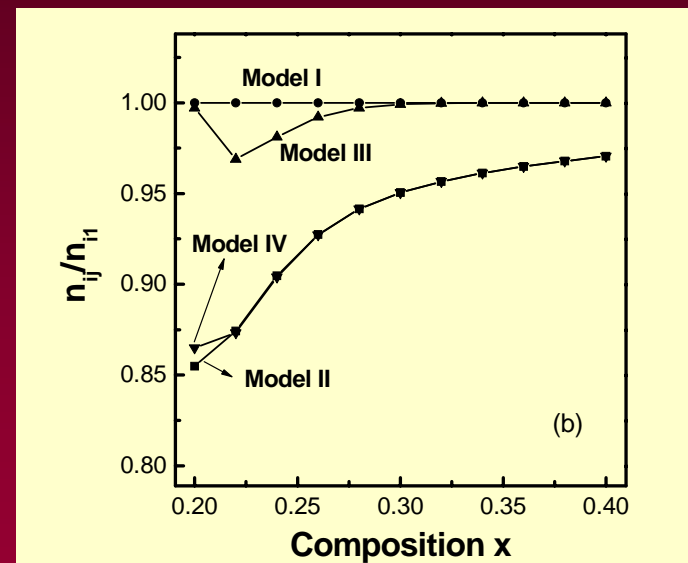
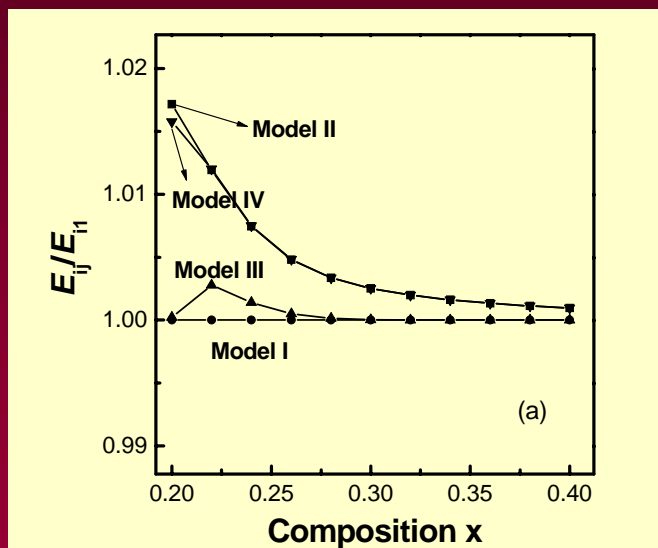


Fig. 4. Relative deviations of Model II, III and IV against Model I in intrinsic Fermi level E_{ij}/E_{i1} (a) and intrinsic carrier concentration n_{ij}/n_{i1} (b) at various composition x . (subscript $j=1\sim 4$ denotes four models, respectively.)

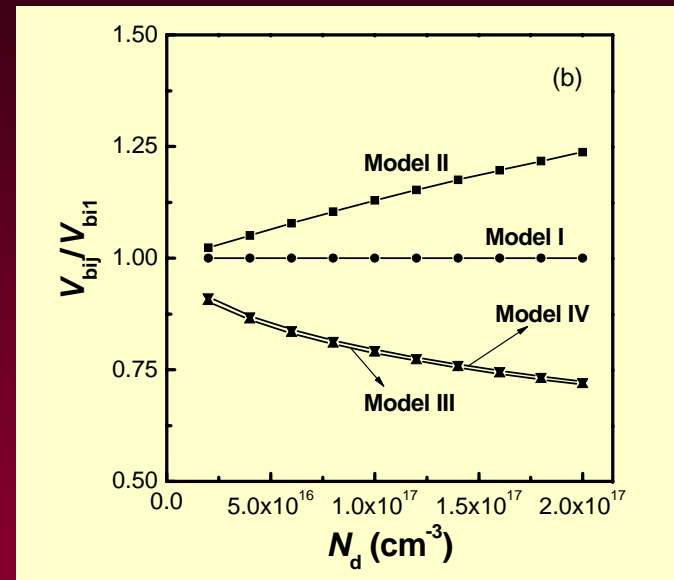
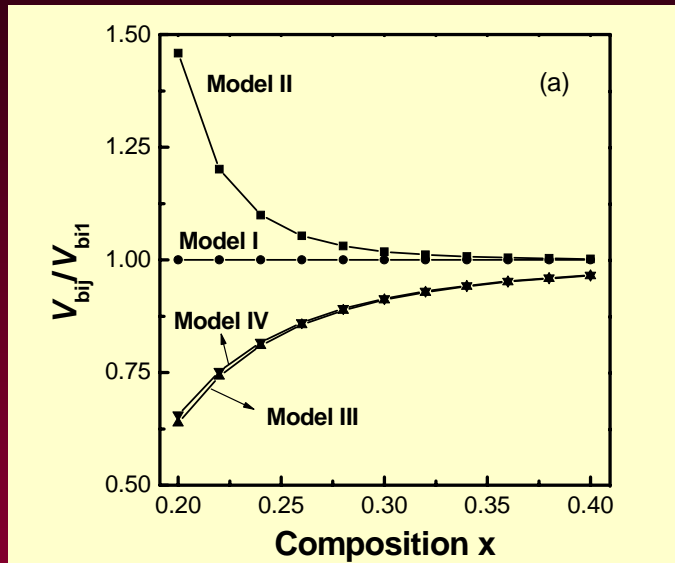


Fig. 5. Relative deviations of Model II, III and IV against Model I in built-in potential V_{bij}/V_{bi1} at various composition x (a) and various n -side doping density N_d (b). (subscript $j=1\sim 4$ denotes four models, respectively.)



In Figure 4(a), the deviations of E_{ij}/E_{i1} from Model I (unity) are less than 2% and might be omitted. In Figure 4(b), the deviations of n_{ij}/n_{i1} from unity increase with the decreasing x , and rise up to 15% at $x=0.2$. V_{bi} is related not only to temperature and composition but also to doping density. Figure 5 shows the plots of V_{bij}/V_{bi1} versus the composition x (a) and the doping density of the n -side, N_d (b). The deviations of V_{bij}/V_{bi1} from unity increase with the decreasing x and increasing N_d .

In conclusion, for SWIR and MWIR with light doping, the effects of carrier degeneracy and conduction band non-parabolicity may be omitted.

For LWIR with light doping or those devices with heavy doping, the omission of carrier degeneracy and conduction band non-parabolicity will lead to enormous error in the calculation of the dark current. By using Model I, an accurate simulation can be obtained.



Fitting method

The measured I - V curves generally include photocurrent due to the background illumination. Based on the assumption of low photon injection, the photocurrent can be regarded as bias-independent. The I - V curve of an illuminated photodiode is described by a linear superposition of the dark current and the bias-independent photocurrent. The R - V curves of illuminated photodiodes are the same as those of unilluminated ones. Therefore, the R - V curves are the fitting object in our fitting process.

$$R_{diff} = \left(\frac{dI_{diff}}{dV_e} \right)^{-1}$$

$$R_{gr} = \left(\frac{dI_{gr}}{dV_e} \right)^{-1}$$

$$R_{tat} = \left(\frac{dI_{tat}}{dV_e} \right)^{-1}$$

$$R_{bbt} = \left(\frac{dI_{bbt}}{dV_e} \right)^{-1}$$

$$R_{fit} = \left(\frac{1}{R_{diff}} + \frac{1}{R_{gr}} + \frac{1}{R_{tat}} + \frac{1}{R_{bbt}} \right)^{-1} + R_s$$



In our fitting procedure, the algorithm is to minimize the function

$$F = \sum_{i=1}^N \left[\log(R_{fit}(V_{di})) - \log(R_{exp}(V_{di})) \right]^2$$

For planar n-on-p photodiodes fabricated using ion-implantation, six fitting parameters can be extracted as follows: the dopant density N_d in *n*-region, the ratio of mobility to lifetime of electrons μ_n/τ_n in *p*-region, the effective lifetime τ_0 in the depletion region, the relative energy position of trap level E_t/E_g and its density N_t in the depletion region, and the series resistance R_s .

An initial value should be input in for each fitting parameter, and then minimize the fitting variance F by using a standard nonlinear gradient-search method combined with the algorithm of reconstruction of the whole-region-minimum for N-dimensional function .



F function depends on six parameters and has multi-minimum in the six-dimensional space due to the tendency of the algorithm to converge on local minima, the values of the extracted parameters are often different for different initial values.

In addition, it takes much time to fit for a large variation range of the six parameters. Therefore, The main task for improving the fitting method is to carefully determine the initial values of the fitting parameters.

The following equation comes into existence for any bias:

$$R_{\text{exp}} - \left(\frac{1}{R_{\text{diff}}} + \frac{1}{R_{\text{gr}}} + \frac{1}{R_{\text{tat}}} + \frac{1}{R_{\text{bbt}}} \right)^{-1} - R_s = 0$$

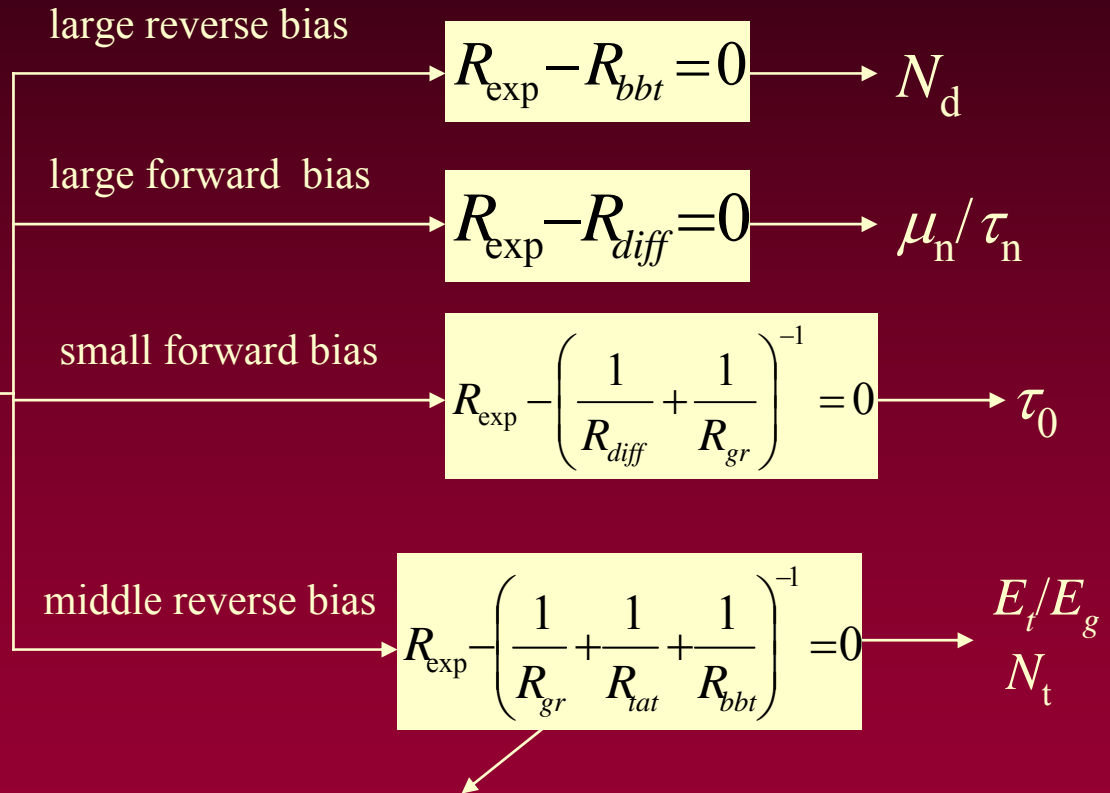
A set of six-variable equations is obtained by choosing six characteristic points on the measured R - V curve.



For long-wavelength MCT diodes, I_{diff} dominates the dark current under large forward bias.

$$R_{exp} - \left(\frac{1}{R_{diff}} + \frac{1}{R_{gr}} + \frac{1}{R_{lat}} + \frac{1}{R_{bbt}} \right)^{-1} - R_s = 0$$

The series resistance R_s , which is comparable to the junction resistance just only under large forward bias, can be omitted in the initial value determination.



A two-variable equation, which can be solved with two of the measured points in the middle reverse bias region, respectively.



Error analysis for extracted parameters

Assuming that this error is effectively resulted from one of the six fitting parameters, this parameter's error can be given as

$$\sigma_{x_j} = \left| \frac{\partial R_{fit}}{\partial x_j} \right|^{-1} \cdot \Delta R$$

Four types of dark current mechanisms have different contributions to the dark current under different biases. We can define a criterion of sensitivity:

$$\eta = \left| \frac{\partial R_{fit}(V_d)}{\partial x_j} \cdot \frac{1}{R_{fit}(V_d)} \right|$$

The larger the value of η is, the greater the influence to the corresponding fitting parameter is. The average of σ for those biases, under which η is larger than half of its maximum, is taken as the theoretical estimation error for the specific parameter x_j .



To demonstrate the determination process of the fitting parameters errors and to verify its applicability, some artificial R - V curves, with the combination of the generated noise current and the calculated current with pre-assigned fitting parameters, are fitted as the experimental data by our fitting program.

The differences between the fitting parameters obtained from the fittings and the pre-assigned ones are defined as the real errors.



Table I. Material and device parameters, which are not used as fitting parameters, for calculating the R_d - V curves in Fig. 1

x	T (K)	A (μm^2)	N_a (cm^{-3})	μ_p (cm^2/Vs)
0.233	77.4	784	8×10^{15}	633

Table II. Comparisons of the assigned values of the six fitting parameters and the fitting results of the theoretically generated R - V curves whose noise level is 1%, 2%, and 3%, respectively. (Data in brackets are the standard errors of the results from ten fits in different fitting paths)

	N_a (cm^{-3})	μ_n/τ_n (cm^2/Vs^2)	τ_0 (ns)	E_t/E_g	N_t (cm^{-3})	R_s (Ω)
Assigned	1.676×10^{16}	9.51×10^{13}	0.207	0.491	1.968×10^{12}	200
Noise 1%	1.683×10^{16} (6×10^{12})	1.05×10^{14} (1×10^{12})	0.192 (0.001)	0.4889 (0.0004)	1.988×10^{12} (1×10^{10})	205.2 (0.2)
Noise 2%	1.677×10^{16} (5×10^{12})	9.92×10^{13} (9×10^{11})	0.1834 (0.001)	0.4866 (0.0003)	2.028×10^{12} (9×10^9)	204.2 (0.2)
Noise 3%	1.667×10^{16} (3×10^{12})	1.008×10^{14} (3×10^{11})	0.1843 (0.0003)	0.4869 (0.0001)	1.962×10^{12} (3×10^9)	204.6 (0.1)

It can be seen from Table that when the noise level is smaller than 3%, both the deviation of the fitting results from the assigned ones and the discreteness among the results from the ten fits in different fitting paths are very small.

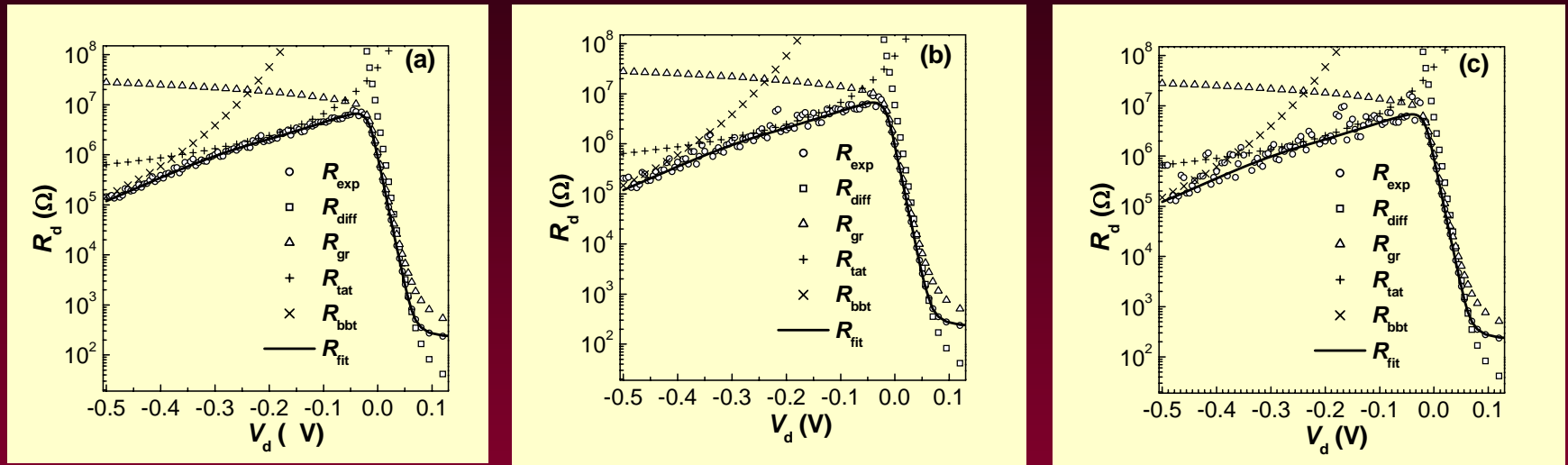


Fig. 6 Fitting results of the artificial R - V curves with the generated noise level of 1% (a), 2% (b), and 3% (c).



As one can see that the largest η for each fitting parameter locates at different bias region, where its related dark current mechanism dominates the dark current.

Accordingly, the estimation error for each fitting parameter can be obtained.

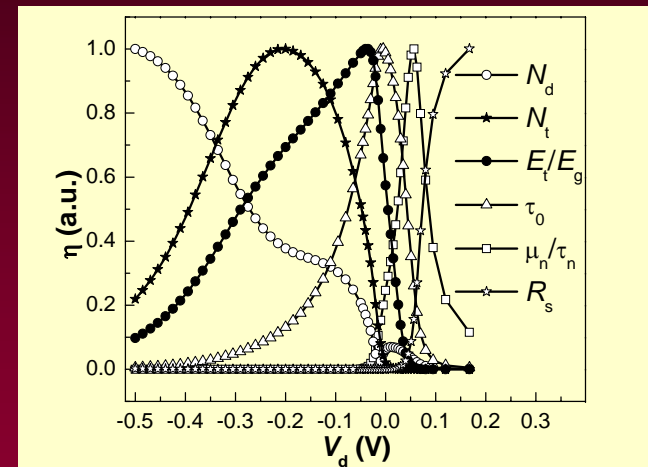


Fig. 7 Normalized sensitivity criterion η versus the bias for the six fitting parameters



Table III. Error ranges of the six fitting parameters of the theoretical R - V curves whose noise level is 1%, 2%, and 3%, respectively. (Data in brackets are the real errors)

	ΔN_d (cm ⁻³)	$\Delta \mu_n / \tau_n$ (cm ² /Vs ²)	$\Delta \tau_0$ (ns)	$\Delta E_f / E_g$	ΔN_i (cm ⁻³)	ΔR_s (Ω)
Noise 1%	6×10 ¹² ~	1×10 ¹² ~ 3×10 ¹³	0.001 ~	0.0004 ~	1×10 ¹⁰ ~	0.2 ~
	9×10 ¹⁴		0.022	0.0051	2.4×10 ¹¹	5.8
	(7×10 ¹³)		(0.015)	(0.002)	(2×10 ¹⁰)	(5.0)
Noise 2%	5×10 ¹² ~	9×10 ¹¹ ~ 3×10 ¹³	0.001 ~	0.0003 ~	9×10 ⁹ ~	0.2 ~
	2.6×10 ¹⁵		0.038	0.014	7.5×10 ¹¹	5.4
	(1×10 ¹³)		(0.024)	(0.0044)	(6×10 ¹⁰)	(4.0)
Noise 3%	3×10 ¹² ~	3×10 ¹¹ ~ 3×10 ¹³	0.0003 ~	0.0001 ~	3×10 ⁹ ~	0.1 ~
	7.2×10 ¹⁵		0.081	0.034	2.0×10 ¹²	5.3
	(9×10 ¹³)		(0.023)	(0.0041)	(6×10 ⁹)	(5.0)

The error range of the fitting parameters can be defined as follows, the standard error of the ten fits in different fitting paths is regarded as the minimum possible error.

It is taken as the lower limit. The estimation error is regarded as the maximum possible error -- the upper limit.

All the real errors drop between the upper and lower limits. This indicates that the estimation errors calculated using this method can be used to represent the accuracy of the fitting parameters.



Application

To verify the applicability of the above developed fitting procedure, the R - V curves of three long-wavelength devices A, B, and C with different Cd composition have been studied.

Table IV. Material and device parameters, which are not used as fitting parameters, for the R_d - V curves of the real devices A, B, and C

Sample	x	T (K)	A (μm^2)	N_a (cm^{-3})	μ_p (cm^2/Vs)
A	0.233	77.4	784	7.69×10^{15}	1290
B	0.2323	77.3	784	9.03×10^{15}	622
C	0.224	77.0	784	8.92×10^{15}	828



Table V. Six fitting parameters of N_d , μ_n/τ_n , τ_0 , E_t/E_g , N_t , and R_s and their error ranges extracted from the measured R - V curves of the real devices A, B, and C. (Data in brackets are the error ranges)

Sample	N_d (cm ⁻³)	μ_n/τ_n (cm ² /Vs ²)	τ_0 (ns)	E_t/E_g	N_t (cm ⁻³)	R_s (Ω)
A	1.79×10 ¹⁶	4.258×10 ¹³	0.0796	0.4524	3.68×10 ¹²	395.5
	(2×10 ¹³ ~ 3×10 ¹⁴)	(3×10 ¹² ~ 6×10 ¹³)	(0.001 ~ 0.02)	(0.0007 ~ 0.006)	(4×10 ¹⁰ ~ 3×10 ¹¹)	(1 ~ 14.8)
B	1.701×10 ¹⁶	1.238×10 ¹⁴	0.1248	0.5008	2.31×10 ¹²	388.2
	(5×10 ¹² ~ 4.5×10 ¹⁴)	(2×10 ¹² ~ 1.2×10 ¹⁴)	(0.0007 ~ 0.04)	(0.0003 ~ 0.005)	(1×10 ¹⁰ ~ 2.3×10 ¹¹)	(0.4 ~ 18.1)
C	2.109×10 ¹⁶	1.024×10 ¹⁵	0.0325	0.4601	8.49×10 ¹⁰	498.7
	(3×10 ¹² ~ 9×10 ¹⁴)	(2×10 ¹⁴ ~ 1.3×10 ¹⁵)	(0.003 ~ 0.005)	(0.005 ~ 0.006)	(5×10 ⁹ ~ 1.9×10 ¹¹)	(2.1 ~ 41.6)

By comparing with the value of the corresponding parameters, the lower limits of the error ranges are very small for all the samples. These data indicate that the discreteness among the results from the ten fits in different fitting paths is very small.

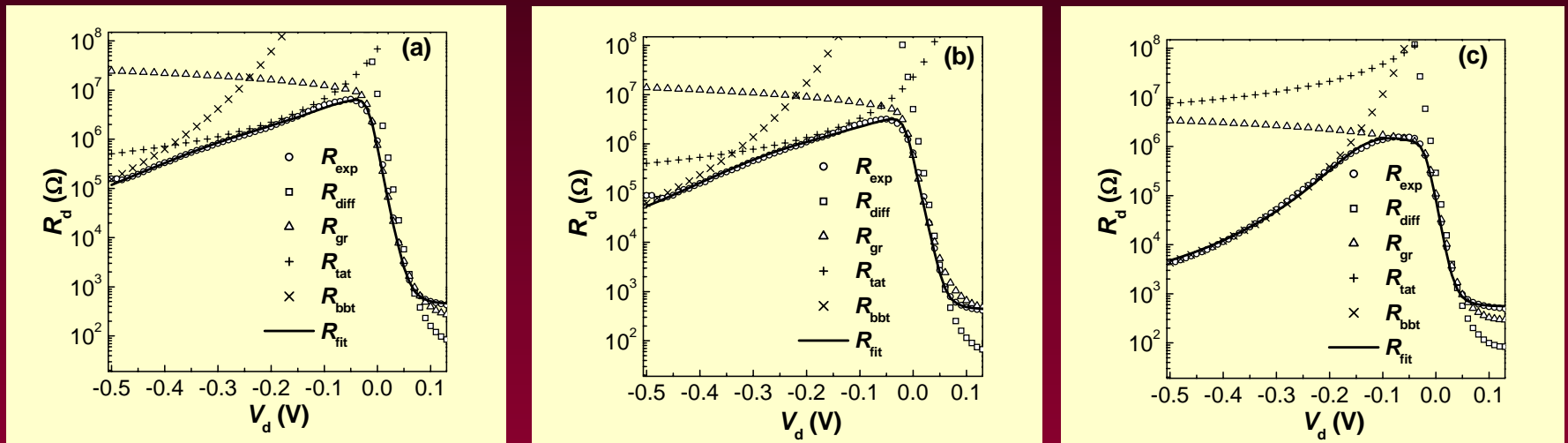


Fig. 8 Measured R - V curves of three real devices and their fitting results for Samples A (a), B (b), and C (c).



In Fig.3, when I_{diff} has only a bit larger contribution to the dark current than I_{gr} after $V_d > 0.05\text{V}$, the effect of series resistance arises and enlarges the estimation error.

The upper limits of the error ranges of N_t for Sample C is twice as much as the value of N_t , since the trap-assisted tunneling current mechanism, which is correlated with the parameter N_t , fails to become dominant under any biases.

Nevertheless, one can see in Fig.3 that the calculated R - V curves accurately fit the measured curves for all the three samples.

Moreover, our fitting method can also correctly fit the specific case like Sample C, for which both the diffusion current mechanism and the trap-assisted tunneling current mechanism fail to be the dominant dark current at any bias in measured R - V curve.



Fitting at different temperature

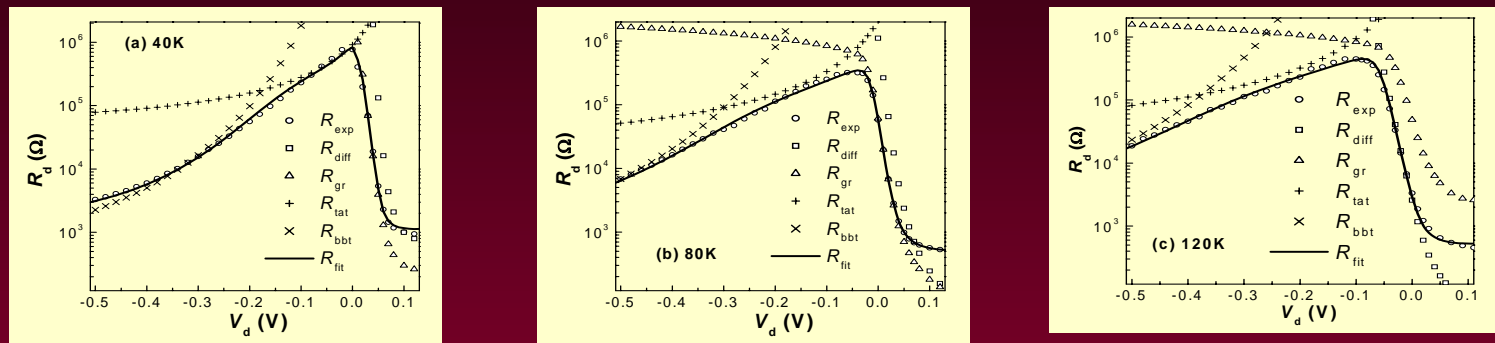
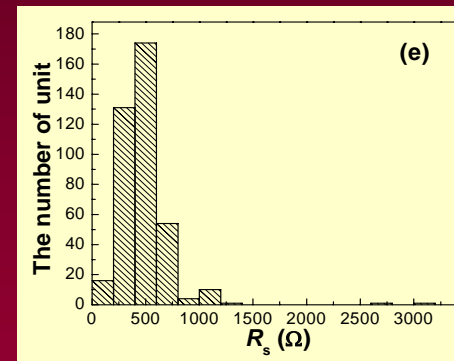
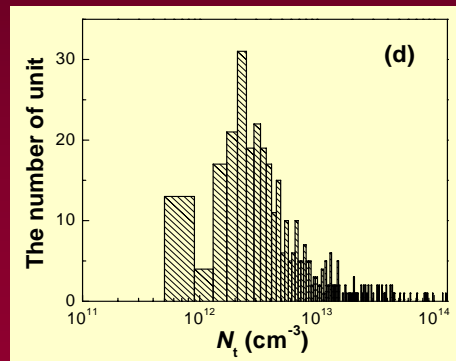
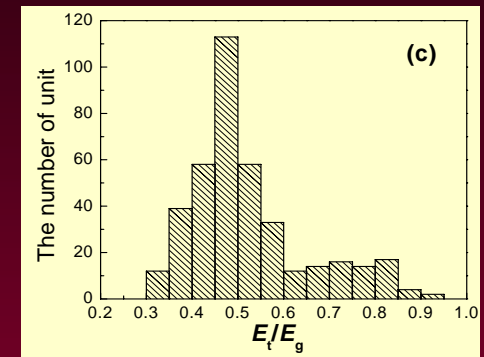
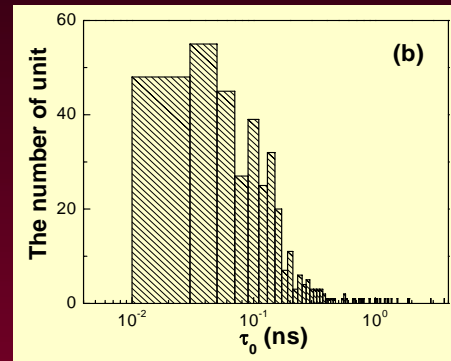
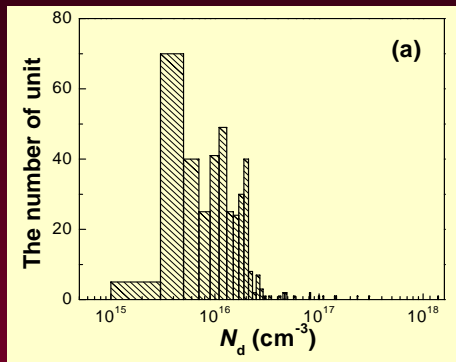


Fig. 9 Fitting results of the curves at 40K (a), 80K (b) and 120K (c).

The calculated R - V curves accurately fit the measured ones at different temperatures. The generation-recombination current (I_{gr}) dominates the dark current at forward bias for low temperature (9a), and the diffusion current (I_{diff}) is the dominant current at forward bias for high temperature (9c). The fitting method can correctly fit the R - V curves measured at different temperature and explore various current limiting mechanisms.



Statistical study



Long-wavelength MCT n-on-p photodiodes in the total 392 samples. Six fitting parameters can be extracted from the measured R-V curves, the dopant density N_d in n-region, the ratio of mobility to lifetime of electrons μ_n/τ_n , the effective lifetime τ_0 , the energy position of trap level E_t/E_g and its density N_t , and the series resistance R_s .



Conclusions

For LWIR with light doping or those devices with heavy doping, the omission of carrier degeneracy and conduction band non-parabolicity will lead to enormous error in the calculation of the dark current.

The fitting method can correctly fit the R - V curves measured at different temperature and indicates various current limiting mechanisms.

By comparing the results of the six parameters, the fitting method developed has highly fault-tolerant capability and could be used as an effective tool to analyze the R - V curves of long-wavelength HgCdTe n-on-p photodiodes.



Shanghai Institute of Technical Physics

Thanks !